

Chapter 2

Cognitive Methods for Semantic Image Analysis in Medical Imaging Applications

In the first part of this chapter, we will briefly discuss the foundations of selected imaging techniques making use of computed tomography (CT). We will focus on dynamic CT perfusion (CTP) and computed tomography angiography (CTA). Later, we will discuss some fundamentals of cognitive computer image analysis aimed at computer-aided diagnosis and semantic image description.

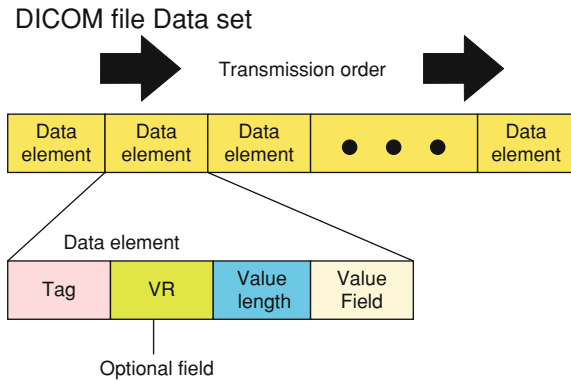
2.1 DICOM Standard

The Digital Imaging and Communications in Medicine Standard (DICOM) addresses multiple levels of the ISO OSI network model and provides support for the exchange of information on interchange media [1]. Its independence of the underlying network technology allows DICOM to be deployed in many functional areas of application, including but not limited to communication via Ethernet, virtual private networks, over dial-up, or other remote access connections. At the application layer, the services and information objects address five primary areas of functionality [1]:

- transmission and persistence of complete objects (such as images, waveforms, and documents);
- query and retrieval of such objects;
- performance of specific actions (such as printing images on film);
- workflow management (support of work lists and status information);
- quality and consistency of image appearance (both for display and print).

Commonly digitalized CT images constituting medical data are stored in DICOM Files [2]. A DICOM File is a file whose content is formatted according to the requirements of the DICOM Standard. In particular, such files contain File Meta Information and a properly formatted dataset. The dataset consists of data elements. Each data element is made up of the following fields:

Fig. 2.1 Schema of a DICOM data set structure consisting of multiple data element structures



- Data Element Tag representing the Group Number followed by the Element Number;
- Value Representation (VR)—only present in the two Explicit VR Data Element structures, it will not be discussed here;
- Value Length—containing the Explicit Length of the Value Field (or an Undefined Length in some special cases);
- Value Field—An even number of bytes containing the Value(s) of the Data Element.

Figure 2.1 presents a schema of the DICOM dataset structure that consists of multiple data element structures.

The information stored in the data element might, for example, comprise the date and time of data acquisition, the type of acquisition device, the imaging protocol, scaling parameters between digital image and real-world size, etc. Knowing the scaling parameters, we can measure the visualized structures for diagnostic purposes. Because of the DICOM file structure, dataset schema information about a particular patient will not be separated from his or her medical data.

2.2 Medical Practice in Computed Tomography Image Interpretation

Since its clinical introduction in 1991, volumetric CT scanning using spiral scanners has resulted in a revolution in diagnostic imaging [3]. In general terms, the capabilities of spiral CT can be expanded in various ways:

- to scan anatomical volumes with standard techniques at significantly reduced scan times,
- to scan larger volumes previously not accessible in scan times,
- to scan anatomical volumes with a high axial resolution (narrow collimation) to closely approach the isotropic voxel of high-quality datasets for excellent 3-dimensional post processing and diagnosis.

Computed tomography was the first diagnostic method that enabled the central nervous system (CNS) to be directly imaged. CT is often the first treatment of a patient with suspected CNS pathology, regardless of the fact that different tomography methods like Magnetic Resonance Imaging (MRI), Single-Photon Emission-Computed Tomography (SPECT), Positron Emission Tomography (PET) have already been introduced. The introduction of multidetector row-computed tomography (MDCT) has greatly improved the diagnostic capabilities of CT in neuroradiology. This applies mainly to examinations of the vascular structure, brain perfusion as well as the diagnosis of patients after trauma. Modern CT also 2D slices along any plane to be reconstructed at a resolution close to that of axial slices. It is also possible to create three-dimensional models of internal organs. If a radiocontrast agent is administered, it is possible to use CT to generate CTA images and computed tomography perfusion (CTP) maps.

The data generated by a contemporary CT scanner consists of a set of two-dimensional axial slices separated by some interslice distance. Each voxel in a slice represents a single Hounsfield unit value (normally 12-bit) of the tissue present inside a given volume. The Hounsfield unit (HU) scale is a linear transformation of the original linear attenuation coefficient measurement into one in which the radiodensity of distilled water at standard pressure and temperature (STP) is defined as zero, while the radiodensity of air at STP is defined as $-1,000$ HU [4]. Hounsfield units are used in medical imaging to describe the amount of X-ray attenuation of each voxel in the 3D image. In practice, these values are arranged on a scale from $-1,024$ to $+3,071$ HU, calibrated so that $-1,024$ HU is the attenuation produced by air and 0 HU is that produced by water, -120 by fat, $+40$ by muscle, and $+400$ or more by bone. The Hounsfield number of a tissue varies according to the density of the tissue; the higher the number, the denser the tissue. While describing CT images, a radiologist uses their knowledge of healthy human anatomy and known symptoms of various illnesses that they learned in their medical practice. Various applications provide them with two- and three-dimensional reconstructions of acquired data, volume measurements of tissues of interest, and HU values in a selected voxel or region. These descriptions, often accompanied by the results of other medical examinations, are used for the final diagnosis. Figure 2.2 presents several axial CT images (a fragment of a bigger volume) acquired for a single patient. Figure 2.3 shows a three-dimensional reconstruction with direct volume rendering of the same CT volume as in Fig. 2.2 [5–8]. We will discuss the direct volume reconstruction technique in Chap. 4 of this book.

2.3 Dynamic CT Perfusion Examination in Diagnostic Evaluation

Computed tomography perfusion (CTP) makes it possible to visualize structural, dynamic, and functional irregularities caused by ischemia, unlike CT which only shows static images of a patient's tissues. In neuroradiography, perfusion image

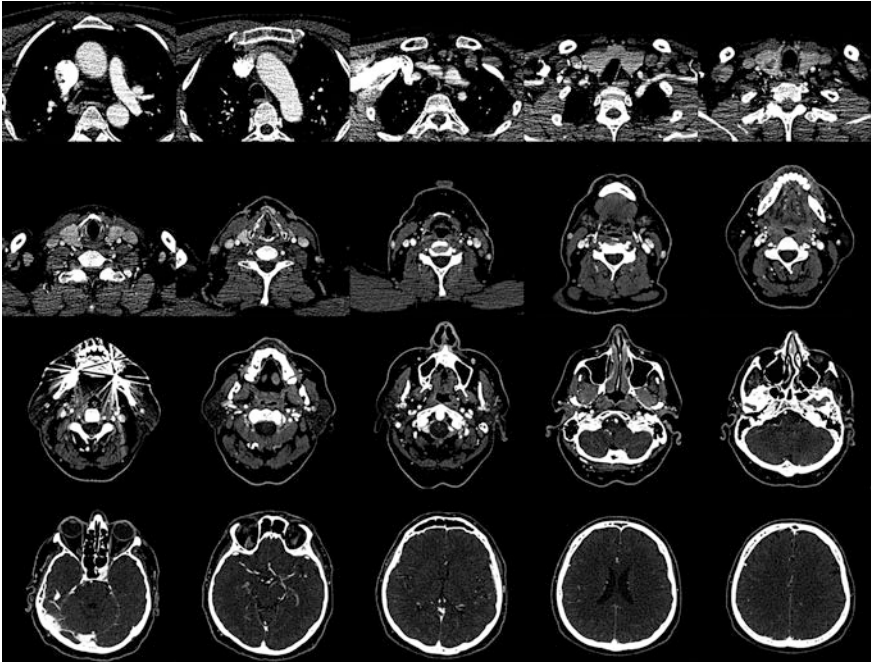


Fig. 2.2 Several CT images acquired for a single patient (the whole dataset includes 414 images). Pixels that represent voxel values are colored proportionally to HU (tissues with low HU values are *dark*, dense tissues are *white*)

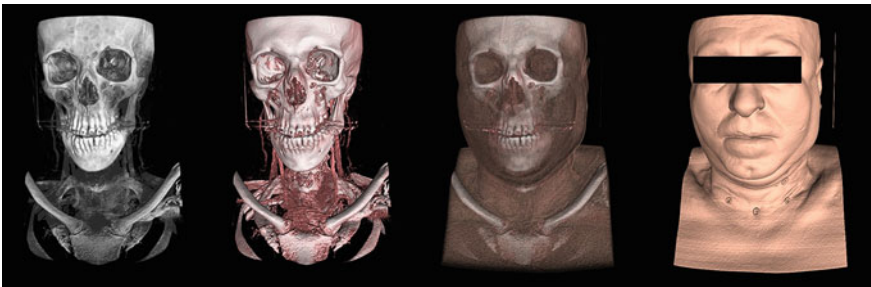


Fig. 2.3 A three-dimensional reconstruction made using the direct volume rendering technique of the same CT volume with a different range of densities enhanced by RGBA color values. From *left* pixels that represent voxel values colored proportionally to HU values (tissues with low HU values are *dark* and nearly transparent, dense tissues are *white* and opaque); bones and blood vessels are enhanced; opaque bones and semi-transparent skin and finally opaque skin (the identity of the person is hidden)

analysis (the terms “perfusion maps” and “perfusion images” are popularly used as equivalents) is currently used in cases of head injuries, epilepsy, vascular brain diseases, and especially to diagnose strokes [9] and brain tumors [10]. The basic principle of perfusion imaging is the repeated scanning of the same brain area while an intravenously injected bolus of a contrast agent passes through the patient’s brain. The obtained scans must then be postprocessed to determine the set of quantity parameters, which are visualized in perfusion maps. The analysis of perfusion examination results (perfusion maps) is based on evaluating parameters important from a medical point of view. The most notable parameters are:

- CBF (cerebral blood flow)—the amount of blood (ml) that flows through 100 g of brain tissue in 1 min;
- CBV (cerebral blood volume)—the volume of blood (ml) that resides in cerebral capillaries and venules per 100 g of tissue;
- MTT (mean transit time)—the average time of contrasted blood flow through brain vascularity;
- TTP (time-to peak)—numbers proportional to the time until the bolus peak is reached, so higher numbers mean later bolus arrival.

2.3.1 Mathematical Model

A number of techniques have been developed during the past decades to evaluate cerebral perfusion [11]. The oldest used is Xe, a lipophilic radioactive tracer that easily diffuses through the blood–brain barrier. Stable xenon CT, however, requires excellent collaboration from the patient, as well as specialized and expensive equipment. It may occasionally be responsible for a decrease in the respiratory rate (yet without reported respiratory failure), headaches, nausea, vomiting, and convulsions [11].

The commonly used method for estimating brain perfusion parameters with CT is dynamic perfusion computed tomography. The theoretical basis of CT CBF measurement technique consists in the central volume principle, first discussed by Meier and Zierler [12], and later extended by Roberts and Larson [13]. Owing to the different possible path lengths that can be followed, blood elements flowing through the capillaries network of the brain will require different lengths of time (transit times) to travel from the arterial input to the venous outlet [14]. The average of all possible transit times through this capillary network is the MTT. The central volume principle relates CBF, CBV, and MTT in the following simple relationship:

$$\text{CBF} = \frac{\text{CBV}}{\text{MTT}} \quad (2.1)$$

In order to apply (2.1), we have to make the blood flow visible to a CT scanner. We can do this by injecting contrast material into the bloodstream. It is also

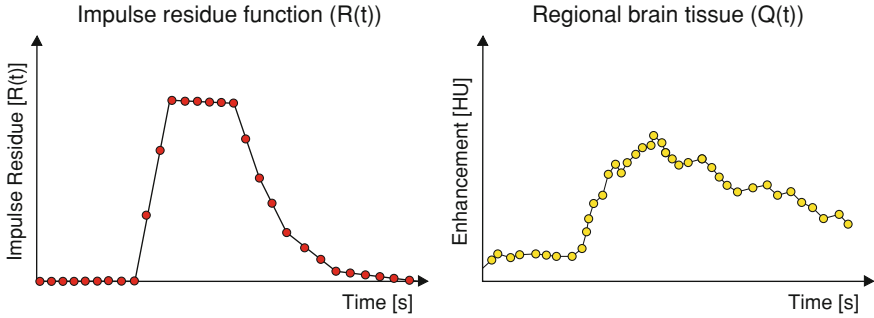


Fig. 2.4 On the left the hypothetical shape of the Impulse residue function $R(t)$ obtained after the deconvolution $C_A(t)$ and $Q(t)$ from Eq. 2.3. On the right a hypothetical regional brain tissue, $Q(t)$ (open circles), a contrast-enhancement curve obtained from CT scanning

assumed that a linear relationship exists between the enhancement in HU numbers and the concentration of the contrast material within an artery or brain tissue region, and that contrast material and blood have the same hemodynamic properties [14].

The contrast material is injected as a bolus of a very short duration. Theoretically, a CT scanner should allow us to observe an enhancement curve with an initial flat plateau followed by a continuous decrease toward the zero baseline (Fig. 2.4 left). This is the so-called Impulse residue function ($R(t)$).

$R(t)$ describes the fraction of the contrast medium remaining in the tissue as a function of time, due to a unit input impulse of the contrast medium [15]. The duration of the plateau corresponds to the time interval during which all the injected contrast material remains in the capillary network [14]. After this time interval, the contrasted blood begins to leave brain vascularity, and the value of $R(t)$ decreases. When $R(t)$ is known, we can use it to compute the MTT according to given formula:

$$MTT = \frac{\int_0^{\infty} R(t) dt}{R_{\max}} \quad (2.2)$$

However, $R(t)$ cannot be directly determined by CT scanning because it is difficult to identify the specific arterial inlet(s) of a brain region [14]. To overcome this problem, Meier and Zierler proposed the following formula [12]:

$$Q(t) = CBF \cdot [C_A(t) \otimes R(t)] \quad (2.3)$$

where $Q(t)$ is the tissue enhancement curve, $C_A(t)$ is the arterial enhancement curve, and \otimes is a convolution operator. On the right side of Fig. 2.4, a hypothetical regional brain tissue ($Q(t)$) contrast-enhancement curve obtained by CT scanning is presented ($C_A(t)$ is similar in shape) (Fig. 2.5).

According to [16], the volume of blood passing through brain vascularity (CBV) can be estimated as

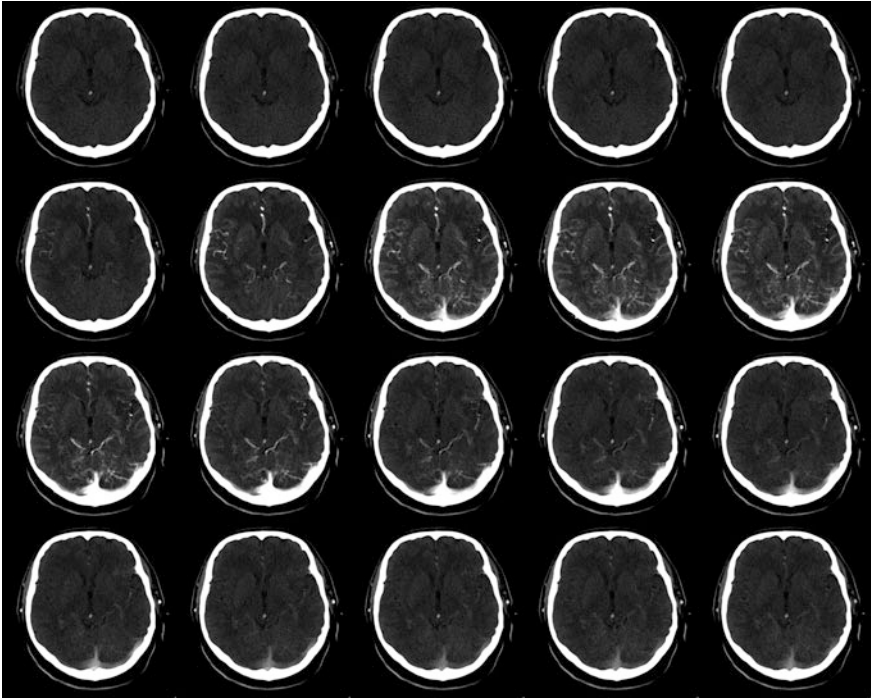


Fig. 2.5 An example set of 20 axial slices (the whole set consisted of 40). The slices are in order row by row from *left to right*. As can be seen while time passes the hyper-intense regions appear enhancing the vascularity of the brain with contrast material that arrived to them

$$\text{CBV} = \frac{\int_0^{\infty} Q(t)dt}{\int_0^{\infty} C_A(t)dt} \quad (2.4)$$

The models (2.1)–(2.4) can be applied successfully only if the blood–brain barrier is intact and there are no recirculations of contrast material [16]. In cases in which the blood–brain barrier is compromised, $Q(t)$ would be the summation of the enhancement due to the contrast material in both the intravascular and extravascular spaces, and CBV would be overestimated. To eliminate the effect of recirculation, the procedure proposed in [14] can be applied. Finally, in order to determinate the CBF value, the following formula has to be computed:

$$\text{CBF} = \frac{\text{CBV}}{\text{MTT}} = \frac{R_{\max} \cdot \int_0^{\infty} Q(t)dt}{\int_0^{\infty} R(t)dt \cdot \int_0^{\infty} C_A(t)dt} \quad (2.5)$$

In order to designate $R(t)$ with the Meier–Zierler model, the $Q(t)$ and $C_A(t)$ values in each sample of TDC must be known. $Q(t)$ can be read directly from a CT scan. In order to measure $C_A(t)$, the common practice is to choose the right artery (or several arteries) in particular the axial slice. This can be done manually [17] or with the help of automatic methods [18]. To compute $R(t)$ using (2.3) the impulse residuum function has to be obtained with the deconvolution (the inverse operation to a convolution). A singular-value-decomposition-based deconvolution technique is often reported as a way to solve this problem [15, 16, 19].

In some cases $C_A(t)$ curves are additionally fitted to the gamma function (the gamma—variate function, [18, 20]). It is done to denoise and eliminate tracer recirculation:

$$Q_\gamma(t) = K \cdot (t - t_0)^\alpha \cdot e^{-\frac{(t-t_0)}{\beta}} \quad (2.6)$$

where t is the time after injection, K is the constant scale factor, α , β , are γ -variety parameters.

Because TTP is the amount of time in which maximal blood flow is reached, the values of pixels in the TTP map can be easily computed pixel-by-pixel by analyzing the deconvolved curves.

2.3.2 Image Acquisition and Post Processing

In a CTP examination, the mass of contrast that remains in the capillary network is measured with a CT scanner. To generate a single set of perfusion maps (CBF, CBV, TPP, and MTT) CTP protocol acquires a series of CT slices in one axial position. A set of pixels that have same image coordinates are used to generate the time density curve (TDC— $Q(t)$). The deconvolution of (2.3) if performed pixel-by-pixel for all TDC curves. All of the examinations last about 40 s and generate 40 slices for each examined axial position. An example set of CT slices from the CTP examination is shown in Fig. 2.5.

In Fig. 2.6, we have presented three perfusion maps generated from the CT time series from Fig. 2.5 by Siemens Syngo Neuro Perfusion CT software. Each perfusion map visualizes a value of a single perfusion parameter and because of that it might be interpreted as a monochrome image. For an easier interpretation by a radiologist they are often additionally colored with a proper lookup table.

Generally, it is emphasized that CTP can provide quantitative data of brain perfusion parameters, which is important in medical data evaluation [19] and can provide valuable diagnostic information. However, the reliability of CTP data with regard to its quantitiveness remains to be established and validated [19]. It has been suggested that the reliability of CTP data depends on the quality of source images, temporal resolution, deconvolution algorithms, the vascular-pixel elimination (VPE) method, and arterial input functions. What is more, perfusion map

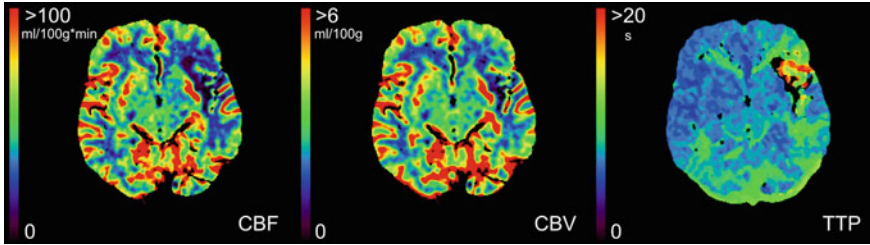


Fig. 2.6 CBF, CBV, and TTP perfusion maps generated from the CT time series from Fig. 2.5. Because CTP maps are grayscale images they are colored with a lookup table that is on the *left* of each figure, for easier interpretation. According to radiologists' description of the CTP maps presented, CBF and CBV are slightly decreased (TTP increased) on the *left* on the level of the *top* sides of the lateral ventricle frontally (the *left* side of the image is on the *right* side of a perfusion image)

generation protocol is not standardized and packages from different vendors might produce different quantity values on CTP maps from the same input data. For example, the perfusion dataset we used in this book for the evaluation of methods (Chap. 3) was generated with Syngo Neuro Perfusion CT by Siemens. We decided to do so because we have not found premises that a particular software is worse or better (more clinically usable) than another.

The assessment of cerebral ischemia by means of perfusion parameters derived from perfusion CT provides valuable information for the prediction of tissue outcome [20]. Also, according to [9, 21–23] a quantitative analyses of the severity of ischemic lesions might be implemented into the diagnostic management of stroke patients.

2.3.3 Prognostic Significance of Cerebral CTP

A great deal of medical research has been done in order to determine a correlation between the values of perfusion parameters and long- and short-term prognoses for examined brain tissues. Despite some minor differences, the authors determined the average value of CBF for health brain tissues as:

$$\overline{CBF}_A \approx 55 \frac{\text{ml}}{100 \text{ g} \cdot \text{min}} \quad (2.7)$$

and average CBV as

$$\overline{CBV}_A \approx 2.5 \frac{\text{ml}}{100 \text{ g}} \quad (2.8)$$

Table 2.1 Average relative values of perfusion parameters (CBF and CBV) and their interpretation according to the literature

rCBF decrease	rCBV decrease	Interpretation
0.60–0.70		Tissues can be salvaged [24, 27–29]
0.20–0.30		Tissues will eventually become infarcted [24, 27–29]
0.62 ± 0.17	0.78 ± 0.18	Tissues can be salvaged [21]
0.34 ± 0.20	0.43 ± 0.22	Tissues will eventually become infarcted [21]

[24]. The dysfunction of neural cells begins when a CBF value drops below $20 \frac{\text{ml}}{100 \text{ g} \cdot \text{min}}$ [9, 10, 25]. Continuous drops of perfusion in range of $10 \sim 20 \frac{\text{ml}}{100 \text{ g} \cdot \text{min}}$ may affect with cell death in many minutes to hours [9]. CBF of less than $10 \frac{\text{ml}}{100 \text{ g} \cdot \text{min}}$ cannot be tolerated beyond a few minutes before infarction occurs causing permanent brain cell damage [9, 10, 25]. Because of some factors [26] the true CBF and CBV values in individual cases may be underestimated in a manner that is difficult to predict. As the result of this some authors prefer to use relative values of CBF and CBV (appropriately rCBF and rCBV—see Table 2.1). The authors in [26] state that a relative comparison of cerebral blood flow within the corresponding areas of both hemispheres of the brain is possible without any limitations because the error of measurement is the same for both high and low CBF values.

It is possible to detect the perfusion deficit area by CTP before noncontrast CT reveals early ischemic changes [30, 31]. The authors in [23] found that the perfused CBV, as imaged by the CTP, reflect the approximate minimum final infarct size in this clinical setting. As cerebral perfusion pressure falls, precapillary resistance vessels dilate (resulting in increased CBV) to maintain the CBF. Once maximum vasodilatation has been reached, autoregulation fails and the CBF begins to fall. As perfusion pressure continues to fall, there is disruption of cellular metabolism, vascular collapse, and the development of irreversible ischemia happens. In an acute ischemic stroke, collapse of vessels at low CBV is likely to occur only after prolonged, severe reductions in CBF, and continued collapse would be associated with a high probability of producing infarction. An increase in CBV reflects the collateral pathway or autoregulation and a decrease in CBV indicates an unfavorable state [32]. A decrease in CBF is a highly sensitive as well as a specific finding in predicting an infarction [27].

In conclusion, both CBF and CBV have prognostic values in the evaluation of the ischemic evolution [33–39]. In many cases, simultaneous analysis of both CBF and CBV perfusion parameters enables an accurate analysis of the ischemia visualized brain tissues and predicts its further changes permitting not only a qualitative (like CT angiography does) but also a quantitative evaluation of the degree of severity of the perfusion disturbance, which results from the particular type of occlusion and collateral blood. The multimodal CT evaluation (CT, CTP, and CTA) improves the detection rate and the prediction of the final size of the infarction in comparison with the unenhanced CT, CT angiography, and perfusion CT alone [40].

2.4 Computed Tomography Angiography

During the past decade CT angiography has become a standard noninvasive imaging modality for the depiction of vascular anatomy and pathology [41]. CTA is primarily performed for assessing the heart, arteries, or veins. After a contrast medium has been injected, the CT scanner acquires the data when the enhancement in the vessel reaches a predetermined operator selected level. The vessels that the contrast medium has already reached are visualized in CT scans as hyper-intensive (brighter) areas. Enhancing the vessel position helps to further segment the circulatory system.

A complete interpretation of CTA includes a review of the transverse CT sections and, in selected cases, multiplanar/curved reformations, volume renderings, maximum-intensity projections, and other images produced during post processing [42].

In Fig. 2.7 example three-dimensional reconstructions of carotid artery CTA with vascular structures enhanced by a contrast agent are presented.

In Chap. 3, we will discuss different approaches for computer-based enhancing and segmentation postprocessing methods for vascular structures that are visualized with three-dimensional CTA images. This includes vessel-enhancing filtering, region growing-based algorithms, and deformable contour-based approaches [43–46].

2.5 Cognitive Methods in Computer Semantic Image Analysis

Cognitive analysis of medical images was made possible by advanced methods of identifying image semantics, which were created thanks to the development of a field called cognitive informatics within modern computer science. Cognitive informatics is a field that combines topics from both cognitive science and information theory, based on both the mechanisms of computer information processing and imitating processes occurring in human brain.

Cognitive informatics thus covers not only the aspects of using mathematical theories to describe and analyze data or information presented in a distributed form, but also engineering fields as well as informatics, cognitive sciences, neuropsychology, cybernetics, computer engineering, knowledge engineering, and computational engineering.

All research problems coming up in the area of cognitive informatics are aimed at understanding the rules followed by human intelligence and cognitive processes taking place in a person's brain. Understanding how the above processes operate allows their transfer and use for solving engineering problems.

Major applications of cognitive informatics methods include the development of the new generation of information systems (i.e., cognitive information systems),

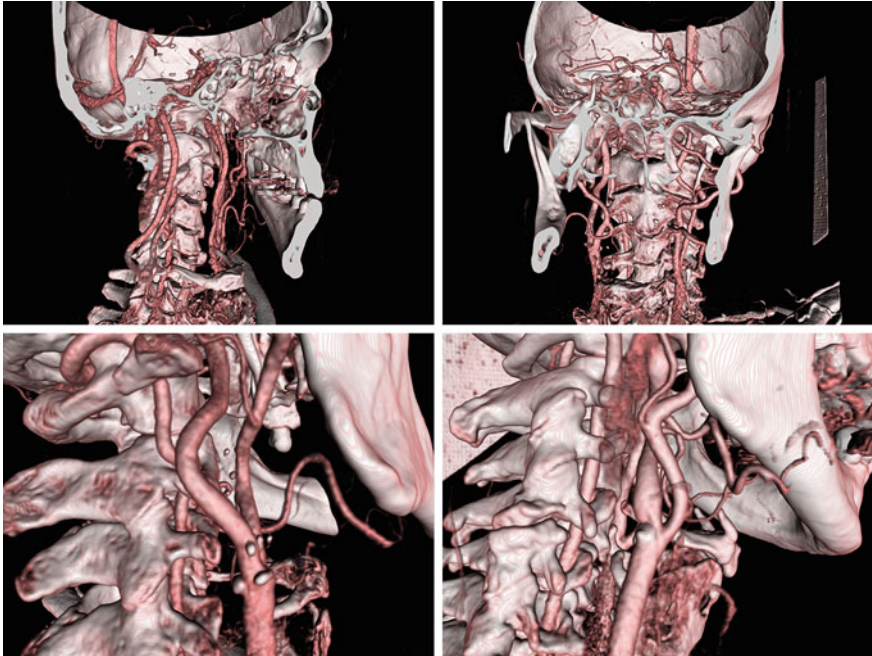


Fig. 2.7 An example three-dimensional reconstruction of a carotid artery CTA with vascular structures enhanced by a contrast agent

the design of cognitive robots, and attempts at the computer analysis of human impressions and sensations, as well as the design of an artificial brain that can perceive, receive, and analyze sensations and impressions. Multiple similar applications also include methods of cognitively analyzing image patterns (including the medical images we are considering) to understand their contents and meaning (semantics).

Similar problems can be solved thanks to the attempt to apply theoretical models of processes occurring in the human brain, associated with activities such as information acquisition, memory modeling, information extraction, or semantic interpretation and information understanding.

In cognitive informatics fields there are many different models allowing for the operation of basic cognitive processes to be identified. These models describe the operation of associational memories, identify methods of learning and perceiving, and also define mechanisms for understanding the world around us. These models are detailed in [52]. The most important of them include the model of information representation in the human brain, the cognitive informatics model built based on the structure of the natural human brain, the natural intelligence model, and the cognitive memory model [52]. However, to allow such biological models solve difficult problems with the use of computers, possible models of cognitive computers were also constructed and enhancements were made to models of cognitive

machines based on cognitive memory models and models of visual perception, which in our case also enables the development of algorithms oriented toward cognitively analyzing medical images.

2.5.1 Cognitive Resonance Model

Semantic (meaning-based) analysis and computer understanding of medical images are made possible by implementing cognitive resonance processes [47–49]. A computer system that conducts this analysis by reference to features characteristic for the specific type of images holds in its base the indispensable knowledge, which allows certain expectations to be generated during the interpretation it carries out. These expectations are generated automatically using the expert knowledge bases collected in the system. Apart from the generated expectations, the information system also carries out an analysis aimed at defining and indicating the appropriate, actual characteristic features of the analyzed data. As a result of combining these significant features describing the analyzed data with expectations generated based on the knowledge held in the system and relating to the semantic contents of the pattern, cognitive resonance occurs [50–52].

Cognitive resonance becomes the cornerstone of the process of understanding the image datasets undergoing analysis. Resonance processes run as described below. The stream of expectations generated by the recognizing system and the stream of features characteristic for the specific dataset are compared, as a result of which certain pairs of expectations and features indicated for the analyzed patterns can increase in importance and others, conversely, decrease in importance. By producing cognitive resonance, this comparison leads to confirming one of the possible hypotheses about the meaning of the pattern, or, on the contrary, demonstrates that the inconsistency of features and expectations is so significant that the hypothesis becomes untrue. The first case means that the analysis process was successful and the semantics of the examined image can be determined, the second means that the attempt to automatically understand the data failed.

In computer systems designed for cognitively analyzing images, cognitive resonance is based on mathematical linguistic methods [50, 51]. The structure of the analyzed image is compared to the structure of data constituting a certain pattern during the recognition process. The comparison is enabled by the strings of the derivation rules of a formal grammar which enable these or similar patterns to be generated unambiguously.

These rules, referred to as productions, are defined in a specially introduced grammar, which in turn defines a certain formal language. Data thus recognized is assigned to the class to which the pattern representing it belongs. In this case, cognitive analysis is based on a syntactic approach which uses additional techniques of processing and analyzing the examined image pattern to determine the semantics of the image. These additional techniques comprise the following operations:

- input image preprocessing;
- analyzing examined object features;
- image coding with picture primitives defined by the introduced formal language.

The completion of such stages makes it possible to re-represent the data in the form of hierarchical structures of a semantic tree and to take subsequent steps of deriving this representation from the initial symbol of the grammar [50, 51].

In a decisive majority of cases, a system carrying out a cognitive analysis while preprocessing image data must segment and identify picture primitives and also determine the relations between them.

The classification proper then consists in recognizing whether the specific obtained linguistic representation of input data belongs to the language generated by the defined formal grammar. Such grammars may come from the classes of sequential, tree, and graph grammars and they are used for recognition during a syntactic analysis conducted by the system [47, 50].

In data analysis processes run by cognitive information systems, a certain significant feature characteristic for these very systems is noted. Processes of semantic image analysis do not have to end at the stage of classifying the analyzed images and recognizing them as belonging to one of the defined classes: they are conducted further, until the image meaning is recognized. This is why cognitive image analysis systems now carry out a stage of automatically understanding the meaning of the image, completed using artificial intelligence technologies, which not only simply recognize but also extract significant semantic information. Only this information allows for the meaning of the image to be interpreted, in other words, supports the full understanding of the image pattern.

Research conducted in this field has led to significant progress in recent years. A number of classes of cognitive vision systems have been proposed for the semantic interpretation of images, including learning-capable E-UBIAS systems described in [49, 52]. The ability of cognitive systems to learn is a very desirable feature. Systems with such capabilities can extend their knowledge base which grows along with the number of semantically interpreted images and which is used to generate system expectations. In such systems, the learning process occurs in five stages.

In the first stage, the semantic information that can be of significance in further analysis process is extracted from sets of possible solutions, so if some information is useless in the current data analysis process, it is treated as superfluous for that process and will be omitted from it. After this stage, the features characteristic for the solution obtained at the first stage of the analysis process are identified. Identifying such features can cause a change in the solution obtained at the first stage, e.g., because the set of expectations or the expert knowledge base is broadened, and thus new patterns are defined.

The next stage focuses on indicating significant changes in the area of characteristic features leading to optimizing the solution formulated, as a result of which the set of characteristic features is redefined in the system.

The last stage of system learning is that of looking for solutions based on a new set of characteristic features and a new expert knowledge base, which at this stage takes the shape of a set of new patterns defined in the cognitive system.

Supplementing data analysis with stages at which the system learns new solutions means that the cognitive resonance must be repeated in the data analysis and image classification process, and if the learning process is multiplied, then cognitive resonance must be repeated more than once.

After the stage at which cognitive systems learn, the analysis and understanding process based on cognitive resonance is repeated, but unlike the traditional analysis process, it now makes use of new (extended) sets of analyzed data and a new base of expert knowledge. It is these very elements that become the primary foundation of cognitive data analysis processes in new systems for image pattern analysis and understanding enhanced with aspects of cognitive system learning.

2.5.2 Semantic Analysis in Cognitive Systems

Methods modeled on cognitive/decision-making processes, particularly those consisting in the description, analysis, and interpretation of the meaning contained in analyzed image datasets play a major role in semantic analysis algorithms. Such processes are inseparably connected with techniques of cognitive analysis, during which a significant role is played by semantic analysis stages. Semantic analysis is thus the key to the correct operation of cognitive data analysis systems. When this analysis is conducted, several different processes occur: interpretation, description, analysis, and semantic reasoning. The main stages in the semantic analysis of images focus on:

- data preprocessing;
- creating the linguistic representation of images, including:
 - recognizing picture primitives;
 - identifying relations between picture primitives;
 - defining relations between objects in the image;
- syntactic pattern analysis;
- pattern classification;
- cognitive resonance;
- determining the semantics of patterns and understanding image data.

Most of the above semantic analysis stages deal with the data understanding process as such, because beginning with the syntactic analysis conducted using the formal grammar defined in the system, tasks are executed to identify the features of the analyzed data with particular focus on its semantics, i.e., the meaning carried by such features.

To properly carry out the computerized process of understanding images, it is necessary to implement feedback techniques during which the features of analyzed

images are compared to expectations generated by the system based on the knowledge it has. Such comparisons are performed using cognitive resonance processes which are crucial for the analysis conducted, i.e., they show the consistency of features and expectations, and the process of data understanding itself, during which the meaning of the analyzed images is identified.

Semantic analysis plays a significant role because it identifies the semantics in the areas within which patterns are interpreted. The proper identification of image semantics is done using the formal grammar, defined in the system, and the set of derivation rules associated with this grammar, which set defines a certain language for describing images and their semantic features. Analysis processes are applied to the features of medical images, which can help interpret diagnostic images [52]. For various classes of medical images, these features may be as follows:

- shape ratios identifying various lesions;
- morphometric values identifying the size, length, and width of the lesion;
- the number of lesions observed (frequently more than one);
- the number of repetitions of the given situation, lesion, pathology;
- the lesion location.

Identifying such lesions allows for a semantic record to be created, which record describes the examined diagnostic image and may also be used at further stages of prognosticating the planned therapy of the diagnosed patient.

2.5.3 Linguistic-Based Cognitive Interpretation of Images

An important aspect of the automatic image understanding method is a very close connection between our methodology and mathematical linguistics, especially a linguistic description of images [52]. There are two important reasons for the selection of linguistic techniques of image description as the fundamental tool for understanding images.

The first one derives from the fact that in the case of understanding we have no limited number of classes or templates known a priori. In fact when we try to understand absolutely an unknown image, the possible number of potential classes goes to infinity. So we must use a tool that offers us possibilities to describe a potentially infinite number of categories. Moreover, the tool under consideration must be constructed from a finite number of elements only, because computers cannot operate using an infinite number of components. This means that it is necessary to have a tool that generates descriptions of classes rather than to point to classes described a priori. For this reason the only suitable tool is a language that can generate an infinite number of sentences on the basis of a finite number of component words in vocabulary and rules in the grammar.

The second reason for using a linguistic method for automatic image understanding is connected with the fact that in the linguistic approach to after image processing, we obtain a description of the image content without the use of any

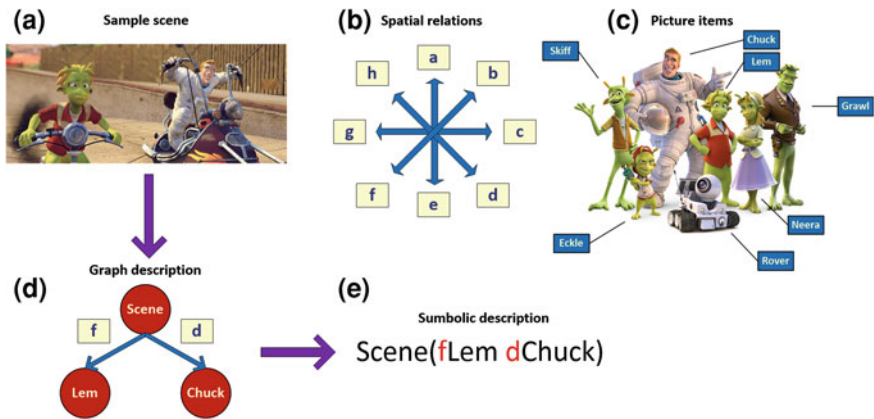


Fig. 2.8 Planet 51 heroes sample scene for syntactic description. **a** Analyzed scene, **b–c** Elements of used vocabulary, **d** Symbolic representation of the scene before describing it in terms of graph-grammar, **e** Conversion of a graph diagram of the image into its symbolic description

classification known a priori due to the fact that even the criteria of the classification are constructed and developed during the automatic reasoning process. This is possible because of a very strong generalization mechanism included into the grammar parsing process. Owing to formal and powerful technologies for the automatic parsing of all linguistic formulas, describing actual images, we can recommend mathematical linguistic methods as the most powerful technology for any pattern generalization. The only problem is connected with a correct adjustment of the terms and methods of formal grammars and languages to the application in the field of images.

When we try to build a language for the description of images we must start with fundamental definitions of elements belonging to the suitable formal grammar. Let us assume that we must build a grammar for the description of a class of scenes similar to the image shown in Fig. 2.8.

An analysis of such a scene shows that we have some classes of graphic objects (‘primitives’), which can be built into the grammar as substantives (nouns). We also have some classes of relations between objects, which can be treated as the verbs of our grammar. So, the vocabulary of grammar for the images under consideration can be shown as in Fig. 2.8b–c.

Using the proposed vocabulary, we can replace the scene with an equivalent scheme for the grammar, as shown in Fig. 2.8d. On the basis of such a symbolic description of the image under consideration we can also use symbolic notations for elements of vocabulary; for every image they obtain a representation in terms of terminal symbols belonging to the definition of the grammar used (see Fig. 2.8e). After a final description of the image, using the elements of a selected image description language, we must implement the cognitive resonance concept. It is, of course, the most difficult part in the whole task. During cognitive

which means that our second hypothesis can now be considered more probable. Yet we are still not quite sure whether the hypothesis is true or not because for its full validation it is necessary to test also other assumptions taken from this hypothesis and from all other hypotheses.

References

1. DICOM (2013) strategic document, version revised in 2013-10-23. <http://medical.nema.org>
2. Digital Imaging and Communications in Medicine (DICOM, PS 3.5-2011) In: Part 5: data structures and encoding, National Electrical Manufacturers Association, 2011. <http://medical.nema.org>
3. Kopp AF, Klingenbeck-Regn K, Heuschmid M, Küttner A, Ohnesorge B, Flohr T, Schaller S, Claussen CD (2000) Multislice computed tomography: basic principles and clinical applications. *Electromedica* 68(2):95–105
4. Celenk C, Celenk P (2012), Bone density measurement using computed tomography. In: Saba L (ed) *Computed tomography—clinical applications*. ISBN: 978-953-307-378-1, doi: [10.5772/22884](https://doi.org/10.5772/22884) (InTech). <http://www.intechopen.com/books/computed-tomography-clinical-applications/bone-density-measurement-using-computed-tomography>
5. Hachaj T, Ogiela MR (2012) Visualization of perfusion abnormalities with GPU-based volume rendering. *Comput Graph-UK* 36(3):163–169. doi:[10.1016/j.cag.2012.01.002](https://doi.org/10.1016/j.cag.2012.01.002)
6. Hachaj T, Ogiela MR (2012). Framework for cognitive analysis of dynamic perfusion computed tomography with visualization of large volumetric data. *J Electron Imaging* 21(4): 043017, doi: [10.1117/1.JEI.21.4.043017](https://doi.org/10.1117/1.JEI.21.4.043017)
7. Hachaj T (2014) Real time exploration and management of large medical volumetric datasets on small mobile devices—Evaluation of remote volume rendering approach. *Int J Inf Manage* 34:336–343. doi:[10.1016/j.ijinfomgt.2013.11.005](https://doi.org/10.1016/j.ijinfomgt.2013.11.005)
8. Hachaj T, Ogiela MR (2010). Augmented reality interface for visualization of volumetric medical data. *Adv Intell Soft Comput* 84:271–277, (Springer, Berlin Heidelberg)
9. Latchaw RE, Yonas H, Hunter GJ, Yuh WTC, Ueda T, Sorensen AG, Sunshine JL, Biller J, Wechsler L, Higashida R, Hademenos G (2003) Guidelines and recommendations for perfusion imaging in cerebral ischemia. *Stroke* 34:1084–1104
10. Hoeffner EG, Case I, Jain R, Gujar SK, Shah GV, Deveikis JP, Carlos RC, Thompson BG, Harrigan MR, Mukherji SK (2004) Cerebral perfusion CT: technique and clinical applications. *Radiology* 231(3):632–644
11. Wintermarka M, Thirana JP, Maedera P, Schnydera P, Meuli R (2001) Simultaneous measurement of regional cerebral blood flow by perfusion ct and stable xenon CT: a validation study. *Am J Neuroradiol* 22:905–914
12. Meier P, Zierler KL (1954) On the theory of the indicator-dilution method for measurement of blood flow and volume. *J Appl Physiol* 6(12):731–744
13. Roberts GW, Larson KB (1973) The interpretation of mean transit time measurements for multi-phase tissue systems. *J Theor Biol* 39(2):447–475
14. Cenic A, Nabavi DG, Craen RA, Gelb AW, Lee TY (1999) Dynamic CT measurement of cerebral blood flow: a validation study. *AJNR Am J Neuroradiol* 20(1):63–73
15. Koh TS, Tan CKM, Cheong LHD, Limc CCT (2006) Cerebral perfusion mapping using a robust and efficient method for deconvolution analysis of dynamic contrast-enhanced images. *NeuroImage* 32(2):643–653
16. Axel L (1980) Cerebral blood flow determination by rapid-sequence computed tomography: a theoretical analysis. *Radiology* 137(3):679–686

17. Wittsack HJ, Wohlschläger AM, Ritzl EK, Kleiser R, Cohnena M, Seitz RJ, Mödler U (2008) CT-perfusion imaging of the human brain: advanced deconvolution analysis using circulant singular value decomposition. *Comput Med Imaging Graph* 32(1):67–77
18. Hirata M, Sugawara Y, Murase K, Miki H, Mochizuki T (2005) Evaluation of optimal scan duration and end time in cerebral CT perfusion study. *Radiat Med* 23(5):351–363
19. Sasaki M, Kudo K, Oikawa H (2006) CT perfusion for acute stroke: current concepts on technical aspects and clinical applications. *Int Congr Ser* 1290:30–36
20. Koh TS, Hou Z (2002) A numerical method for estimating blood flow by dynamic functional imaging. *Med Eng Phys* 24(2):151–158
21. Koenig M, Kraus M, Theek C, Klotz E, Gehlen W, Heuser L (2001) Quantitative assessment of the ischemic brain by means of perfusion-related parameters derived from perfusion CT. *Stroke* 32(2):431–437
22. Eastwood JD, Lev MH, Wintermark M, Fitzek C, Barboriak DP, Delong DM, Lee TY, Azhari T, Herzau M, Chilukuri VR, Provenzale JM (2003) Correlation of early dynamic CT perfusion imaging with whole-brain MR diffusion and perfusion imaging in acute hemispheric stroke. *AJNR Am J Neuroradiol* 24(9):1869–1875
23. Lev MH, Segal AZ, Farkas J, Hossain ST, Putman C, Hunter GJ, Budzik R, Harris GJ, Buonanno FS, Ezzeddine MA, Chang Y, Koroshetz WJ, Gonzalez RG, Schwamm LH (2001) Utility of perfusion-weighted CT imaging in acute middle cerebral artery stroke treated with intra-arterial thrombolysis: prediction of final infarct volume and clinical outcome. *Stroke* 32(9):2021–2028
24. Eastwood JD, Lev MH, Azhari T, Lee TY, Barboriak DP, Delong DM, Fitzek C, Herzau M, Wintermark M, Meuli R, Brazier D, Provenzale JM (2002) CT perfusion scanning with deconvolution analysis: pilot study in patients with acute middle cerebral artery stroke. *Radiology* 222(1):227–236
25. Aksoy FG, Michael HL (2000) Dynamic contrast-enhanced brain perfusion imaging: technique and clinical applications. *Semin Ultrasound CT MR* 21(6):462–477
26. Koenig M, Klotz E, Heuser L (1998) Perfusion CT in acute stroke: characterization of cerebral ischemia using parameter images of cerebral blood flow and their therapeutic relevance. *Clinical experiences. Electromedica* 66:61–67
27. Mayer TE, Hamann GF, Baranczyk J, Rosengarten B, Klotz E, Wiesmann M, Missler U, Schulte-Altdorneburg G, Brueckmann HJ (2000) Dynamic CT perfusion imaging of acute stroke. *AJNR Am J Neuroradiol* 21(8):1441–1449
28. Wintermark M, Reichhart M, Thiran JP, Maeder P, Chalaron M, Schnyder P, Bogousslavsky J, Meuli R (2002) Prognosis accuracy of cerebral blood flow measurement by perfusion computed tomography, at the time of emergency room admission, in acute stroke patients. *Ann Neurol* 51(4):417–432
29. Klotz E, König M (1999) Perfusion measurements of the brain: using dynamic CT for the quantitative assessment of cerebral ischemia in acute stroke. *Eur J Radiol* 30(3):170–184
30. Reichenbach JR, Röther J, Jonetz-Mentzel L, Herzau M, Fiala A, Weiller C, Kaiser WA (1999) Acute stroke evaluated by time-to-peak mapping during initial and early follow-up perfusion CT studies. *AJNR Am J Neuroradiol* 20(10):1842–1850
31. Guan X, Yu X, Liu X, Long J, Dai J (2003) CT perfusion imaging and CT subtraction angiography in the diagnosis of ischemic cerebrovascular disease within 24 hours. *Chin Med J* 116(3):368–372
32. Higashida RT, Furlan AJ, Roberts H, Tomsick T, Connors B, Barr J, Dillon W, Warach S, Broderick J, Tilley B, Sacks D (2003) Technology assessment committee of the american society of interventional and therapeutic neuroradiology; technology assessment committee of the society of interventional radiology, trial design and reporting standards for intra-arterial cerebral thrombolysis for acute ischemic stroke. *Stroke* 34(8):109–137
33. Hachaj T (2012) Pattern Classification Methods for Analysis and Visualization of Brain Perfusion CT Maps. *Comput Intell Paradig Adv Pattern Classif* 386:145–170

34. Hachaj T, Ogiela MR (2010) Automatic detection and lesion description in cerebral blood flow and cerebral blood volume perfusion maps. *J Signal Process Syst Signal Image Video Technol* 61(3):317–328. doi:[10.1007/s11265-010-0454-0](https://doi.org/10.1007/s11265-010-0454-0)
35. Hachaj T, Ogiela MR (2011) Intelligent information system for interpretation of dynamic perfusion brain maps. *Lect Notes Artif Intell* 6591:406–415
36. Hachaj T, Ogiela MR (2011) CAD system for automatic analysis of CT perfusion maps. *Opto-Electron Rev* 19(1):95–103. doi:[10.2478/s11772-010-0071-2](https://doi.org/10.2478/s11772-010-0071-2)
37. Hachaj T, Ogiela MR (2011) A system for detecting and describing pathological changes using dynamic perfusion computer tomography brain maps. *Comput Biol Med* 41(6):402–410. doi:[10.1016/j.combiomed.2011.04.002](https://doi.org/10.1016/j.combiomed.2011.04.002)
38. Hachaj T, Ogiela MR (2011) Augmented reality approaches in intelligent health technologies and brain lesion detection. *Lect Notes Comput Sci* 6908:135–148
39. Hachaj T, Ogiela MR (2013) Application of neural networks in detection of abnormal brain perfusion regions. *Neurocomputing* 122:33–42. doi:[10.1016/j.neucom.2013.04.030](https://doi.org/10.1016/j.neucom.2013.04.030)
40. Kloska SP, Nabavi DG, Gaus C, Nam EM, Klotz E, Ringelstein EB, Heindel W (2004) Acute stroke assessment with CT: do we need multimodal evaluation? *Radiology* 233(1):79–86
41. Yu T, Zhu X, Tang L, Wang D, Saad N (2007) Review of CT angiography of Aorta. *Radiol Clin North Am* 45(3):461–483
42. American College of Radiology (ACR), American Society of Neuroradiology (ASNR)(2010) ACR-ASNR practice guideline for the performance and interpretation of cervicocerebral computed tomography angiography (CTA). [online publication]. Reston (VA), American College of Radiology (ACR), p 7
43. Hachaj T, Ogiela MR (2012) Segmentation and visualization of tubular structures in computed tomography angiography. *Lect Notes Artif Intell* 7198:495–503
44. Hachaj T, Ogiela MR (2012) Evaluation of carotid artery segmentation with centerline detection and active contours without edges algorithm. *Lect Notes Comput Sci* 7465:469–479
45. Ogiela MR, Hachaj T (2012). The automatic two-step vessel lumen segmentation algorithm for carotid bifurcation analysis during perfusion examination. In: Watada J, Watanabe T, PhillipsWren G (eds) *Intelligent decision technologies (IDT'2012)*, vol 2. Smart innovation systems and technologies, vol 16, pp 485–493
46. Ogiela MR, Hachaj T (2013) Automatic segmentation of the carotid artery bifurcation region with a region-growing approach. *J Electron Imaging* 22(3): 033029, doi: [10.1117/1.JEI.22.3.033029](https://doi.org/10.1117/1.JEI.22.3.033029)
47. Ogiela L (2008) Cognitive systems for medical pattern understanding and diagnosis. *Lect Notes Artif Intell* 5177:394–400
48. Ogiela L (2008) Syntactic approach to cognitive interpretation of medical patterns. *Lect Notes Artif Intell* 5314:456–462
49. Ogiela L (2009) UBIAS systems for the cognitive interpretation and analysis of medical images. *Opto-Electron Rev* 17(2):166–179
50. Ogiela L (2010) Cognitive informatics in automatic pattern understanding and cognitive information systems. *Stud Comput Intell* 323: 209–226 (Springer, Berlin Heidelberg)
51. Ogiela L, Ogiela MR (2009). Cognitive techniques in visual data interpretation. *Stud Comput Intell* 228 (Springer, Berlin Heidelberg)
52. Ogiela L, Ogiela MR (2012) *Advances in cognitive information systems*. Cognit Syst Monogr 17 (Springer: Berlin Heidelberg)



<http://www.springer.com/978-3-319-07799-4>

Natural User Interfaces in Medical Image Analysis

Cognitive Analysis of Brain and Carotid Artery Images

Ogiela, M.R.; Hachaj, T.

2015, XII, 288 p. 124 illus., 74 illus. in color., Hardcover

ISBN: 978-3-319-07799-4